Coastal Engineering 168 (2021) 103901

Contents lists available at ScienceDirect

Coastal Engineering

journal homepage: www.elsevier.com/locate/coastaleng

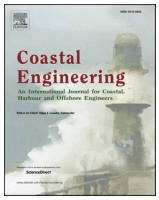

Estimation of layer coefficients of cubipod homogeneous low-crested structures using physical and numerical model placement tests

Jorge Molines [a,*], Riccardo Centi [b], Marcello Di Risio [b], Josep R. Medina [a]

[a] Universitat Politècnica de València,Institute of Transport and Territory, Camino de Vera s/n, 46022, Valencia, Spain
[b] University of L'Aquila, Department of Civil, Construction-Architectural and Environmental Engineering (DICEAA), Environmental and Maritime Hydraulic Laboratory (LIAM), P.le Pontieri, 1 - 67040, Monteluco di Roio, L'Aquila, Italy

ARTICLE INFO

Keywords:
Placement grid
Mound breakwaters
Game engine
Bullet physics engine
Layer coefficient
Cubipod

ABSTRACT

Homogeneous low-crested structures (HLCSs) on hard seabed are designed to protect beaches and regenerate coral reefs. The height of a HLCS depends on the placement grid which determines the crest freeboard, wave transmission and concrete consumption. In real seafloor conditions, it is not easy to define feasible placement grids for HLCSs on uneven sea bottoms. In this study, the parameters of the numerical model Bullet Physics Engine (BPE) are calibrated and validated using the results of small-scale physical model placement tests of five-layer Cubipod HLCSs on horizontal rigid bottom. The BPE model showed a low sensitivity to variations in the calibrated parameters; the numerical model estimated the layer coefficients with global mean relative errors of 1.04% and 1.39% in the triangular and rectangular placements grids, respectively. Once the numerical model was calibrated, new numerical and physical model tests on a 4% rigid bottom slope were compared for validation. A five-layer Cubipod HLCS on a 4% bottom slope was simulated using the BPE numerical model showing a global mean relative error of 2.75% compared to the small-scale physical model tests. A good agreement was found between numerical and physical model tests of five-layer Cubipod HLCSs on both horizontal as well as 4% rigid bottom slope. The BPE numerical model was found a suitable tool to estimate the structure height of HLCSs and to optimize placement grids of HLCSs on real cases with hard sea bottom.

1. Introduction

Coral reefs act as a natural protection against beach erosion and coastal flooding in areas such as the Caribbean Sea (Mesoamerican Barrier Reef System) or Australia (Great Barrier Reef). Coral reefs reduce the wave energy attacking the neighbouring beaches in the short term and generate biogenetic sand in the long term. Climate change, ocean acidification, pollution and other anthropogenic causes are responsible for the global degradation of coral reefs in the world. Rinkewich (2014) estimates coral reefs have been retreating more than 1% annually in the past four decades, and Ferrario et al. (2014) noted that this degradation have been affecting numerous beaches in the world. New measures for the regeneration of coral reefs is a priority to keep the risk of the societies protected by coral reefs under tolerable limits. To this end, Odériz et al. (2018) pointed out that homogeneous low-crested structures (HLCSs) can be an adequate natural-based solution to regenerate retreating coral reefs. HLCSs can withstand intense wave storms providing a stable porous hard substrate to fix the coral larvae while protecting the neighbouring beaches.

For centuries, mound breakwaters have been constructed to shelter harbors and to protect coastal areas. Detached breakwaters parallel to the coast are commonly used for shore protection with the main goal of reducing the wave energy flux on the coastline. Conventional detached breakwaters are low-crested structures (LCSs), submerged or slightly emerged mound breakwaters usually with core, filter and armor layers. Odériz et al. (2018) proposed the construction of HLCSs similar to conventional LCSs but using large rocks or concrete units without core; this typology minimizes the environmental impact and, if necessary, dismantling is easy and the units are re-useable. HLCSs are highly porous structures which favour local biodiversity increasing their value as green infrastructure (Medina et al., 2019) making them adequate to regenerate coral reefs. Retreating coral reef areas usually provide hard seabeds above which a HLCS can be placed; therefore, the settlement of a typical application of a HLCS is negligible. Fig. 1a and b illustrate the

* Corresponding author.
E-mail addresses: jormollo@upv.es (J. Molines), riccardo.centi00@gmail.com (R. Centi), marcello.dirisio@univaq.it (M. Di Risio), jrmedina@upv.es (J.R. Medina).

https://doi.org/10.1016/j.coastaleng.2021.103901
Received 16 February 2021; Received in revised form 29 March 2021; Accepted 2 April 2021
Available online 13 April 2021

cross-section of a conventional LCS and a HLCS, respectively.

The crest freeboard of a HLCS is crucial for estimating the amount of energy transmitted to the shoreline (Medina et al., 2019). However, it is not easy to measure and control the structure height of a HLCS because it depends on the placement grid. Given a hard sea bottom, the placement grid determines the structure porosity and layer thicknesses (Medina et al., 2020) and, contrary to conventional LCSs, structure height of HLCSs decreases if armor porosity increases (De Keyser and Jacobs, 2020). Adequate placement grids for HLCSs are not straightforward and have only received limited attention in the literature.

Small-scale physical model tests using the Froude similarity have been the main source of scientific information for coastal engineers to design mound breakwaters. Small-scale physical model tests usually provide a reliable and realistic response of the structures which are useful for design optimization or validation. However, small-scale physical model tests require special facilities (wave flumes, wave basins, etc.), they are time-consuming and the model and scale effects are always a matter of concern, which may be reduced with the appropriate scale and model layout. The placement grid of the armor layers of conventional mound breakwaters significantly affects the armor porosity, armor stability, wave overtopping, and concrete consumption (Medina et al., 2014). Based on realistic small-scale physical model placement tests, Yagci and Kapdalsi (2003), Özkan-Cèvik (2005), and Pardo et al. (2014) analyzed feasible armor porosities that can be constructed using Antifer, Core-loc, and Cubipod concrete units for breakwater armoring. Realistic physical model placement tests such as those of Pardo et al. (2014) are time-consuming and require special equipment such as small-scale crawler cranes, as well as trained crane operators.

Compared to small-scale physical model placement tests, numerical model placement tests are considered a valuable and competitive tool to analyze the feasibility of placement grids (Latham et al., 2013). The armor unit behavior is usually simulated using: (1) discrete and finite element models (Latham et al., 2008) or (2) rigid body models (Cooper et al., 2008). The first approach is based on the discretization of the structural element into finite or discrete elements and requires a high computational time, while the second approach is based on the second Newton law and requires the use of Physics Engines from the gaming industry (PhysX or Bullet) with a relatively low computational time.

In this study, physical and numerical model placement tests were conducted to simulate different placement grids of Cubipod HLCSs measuring the layer thickness of each layer. The Bullet Physics Engine (BPE) incorporated in the Blender Free and Open 3D Creation Software (Blender, 2019) is used to conduct the numerical model placement tests, validated later with physical model placement tests without water. This study is divided into the following sections. Firstly, a literature review is provided. Secondly, the physical and numerical model placement tests are described. Thirdly, the numerical model placement tests are validated. Fourthly, an application is analyzed. Finally, a summary and some conclusions are given.

2. Literature review

2.1. Physical placement techniques for concrete armor units

Concrete armor units can be uniformly, patterned or randomly placed on mound breakwaters (Dupray and Roberts, 2009). All the armor units, even those which require unit orientation, are placed using a cartesian X–Y grid which allows the crane operator to achieve the desired armor porosity at prototype scale. The placement technique depends on the type of unit, number of layers, armor porosity and interlocking. It is recommended to carry out realistic placement tests in laboratory to optimize placement grids (Medina et al., 2010) and to control the armor unit placement at prototype scale. Unfeasible placement grids or uncontrolled placement may lead to costly conflicts, miscalculations and repair works because armor units can be lost during placement or the actual armor porosity may be lower than prescribed, changing the breakwater hydraulic performance.

Yagci and Kapdalsi (2003) analyzed different placement methods for Antifer cubes and concluded that the placement technique affects armor stability, wave run-up and placement costs. Özkan-Çevik et al. (2005) compared two placement grids for Core-Locs and concluded that random placement was preferable since it had higher armor stability. Muttray et al. (2005) tested two different sling methods to place Xblocs; the method with the sling attached to one leg of the X-shaped showed higher armor stability and easier handling and construction. Pardo et al. (2014) tested different placement grids on trunk and roundheads for Cubipod armored mound breakwaters using a small-scale crawler crane. Considering a double-layer Cubipod armored mound breakwater with target armor porosity of 42%, Pardo et al. (2014) recommended a placement grid in the trunk and roundhead with measured armor porosities $p = 41.3\%$ and $p = 45.4\%$, respectively.

Recently, De Keyser and Jacobs (2020) have conducted physical model placement tests of Cubipod five-layer HLCSs measuring the layer thicknesses corresponding to six different placement grids which affect the layer thicknesses, porosity and structure height of HLCSs. These authors concluded that placement grids with larger horizontal distances among units leaded to lower layer thicknesses, higher prosotities and lower HLCS height; two physical model placement grids (RPG and TPG) were analyzed in section 3.1 of this study.

2.2. Numerical placement techniques

Numerical modeling can be used to analyze the armor porosities and concrete stresses in armor units. The individual armor unit behavior is usually simulated using discrete and finite element models or rigid body methods. The Finite Element Method (FEM) is widely used for modeling stress and deformation of solids while the Discrete Element Method (DEM) is capable of modeling the collision and motion tracking of solids (multi-body interaction). The combined finite-discrete element method (FEMDEM) is used to handle complex deformable shapes; Latham et al. (2008), Xiang et al. (2011), Latham et al. (2013) and Guo et al. (2015), solved the contact mechanics using a distributed contact force approach.

Latham et al. (2008) modeled several armor units using DEM and FEMDEM techniques and Computational Fluid Dynamics (CFD). The authors compared laboratory pull-out tests of cube and X-bloc armor with DEM simulations, concluding that the force distributions and absolute values were similar. The authors concluded that FEMDEM simulations are more versatile than DEM simulations and can give accurate geometry representation whereas the required computational time is much higher. Latham et al. (2013) used FEMDEM techniques to construct a Core-Loc armored mound breakwater. The authors conducted five tests and controlled the packing density, spacing, orientation and contact between elements. Latham et al. (2013) obtained packing densities between 0.59 and 0.63, similar to prototypes, and detected that

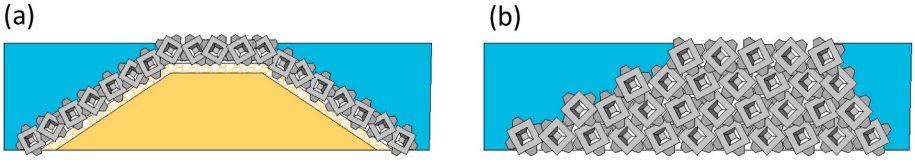

Fig. 1. Cross-section of a Cubipod-armored: (a) conventional LCS, and (b) 4-layer HLCS.

the higher the packing density, the higher the average maximum contact force per unit.

Guo et al. (2015) used a fracture model combined with FEMDEM techniques to investigate the structural integrity of Dolosse and Core-Locs under dynamic and extreme loading conditions. The authors simulated the deformation, fracture initiation and post-fracture behavior of both armor units under drop tests and interactions between armor units on the slope (simulating real mound breakwaters). Anastasaki et al. (2015) used FEMDEM techniques to generate recommendations on the placement grids of Core-loc armor layers. The authors improved the placement protocol reported in Latham et al. (2013) with better representation of the contacts and orientation between units (avoiding units with legs normal to the slope). The first row of units was carefully placed according to technical guidelines (Smith and Melby, 1998). The other armor units were vertically dropped over a slope H:V = 4:3. When the first solid contact occurred, the lowering velocity of the armor unit was set to zero and the friction coefficient between armor units was artificially lowered. To improve the contacts between units, a horizontal vibration together with a slight compaction force was applied. Once the dropped armor unit was in the slope, the friction coefficient between units was increased to ensure a state of equilibrium. Thus, the authors calibrated two friction coefficients, the vibration to improve the settlement and the compaction force. Anastasaki et al. (2015) concluded that both the placement grid and relative orientation between armor units are crucial to achieve the desired packing densities in Core-Loc armored mound breakwaters.

Cooper et al. (2008), Greben et al. (2008), Cooper et al. (2010) and Greben et al. (2010) used the PhysX Physics Engine (a rigid body method) to construct Dolos and Antifer armored mound breakwaters and analyzed the armor stability against oscillatory forces. These authors used a concrete density $\rho = 2\,350$ kg/m^3 but they did not calibrate any of the parameters of the numerical model. They proposed different parameters for the numerical model without any sensitivity analysis or validation. The numerical construction of the armor layers was conducted by sequentially dropping at a constant velocity the armor units and released them when the first contact with the slope appeared following the given placement grid.

Centi (2020) used the Bullet Physics Engine (BPE) to construct Cubipod and Antifer HLCSs. Centi (2020) used a concrete density of $\rho = 2\,300$ kg/m^3 and conducted a sensitivity analysis of some of the parameters of the numerical model within a small range of variation. Centi (2020) measured the layer thicknesses of five-layer Cubipod HLCSs and found a good agreement between the numerical results and the small-scale physical model placement tests carried out by De Keyser and Jacobs (2020).

2.3. Layer thickness

According to USACE (1984), the armor thickness can be calculated as follows:

$$t = nk_{\Delta}D_n \tag{1}$$

where n is the number of layers in the armor, k_{Δ} is the layer coefficient, $D_n=(W/\Upsilon)^{1/3}$ is the nominal diameter, W is the armor unit weight, and Υ is the specific weight. Placing density ϕ(units/m^2), controlled by the placement grid, is related to the layer coefficient (k_{Δ}) and the nominal porosity (P) as detailed in Eq. (2).

$$\phi = nk_{\Delta}\frac{(1-P)}{D_n^2} \tag{2}$$

The dimensionless placing density is the packing density $\phi = \varphi D_n^2$. Frens (2007) pointed out that the different criteria found in the literature to define the layer coefficient caused some misunderstandings; for instance, both USACE (1984) and CIRIA, CUR, and CETMEF (2007) recommend a nominal armor porosity of 50% for double-layer Tetrapod armors, but different layer coefficients, $k_{\Delta} = 1.04$ and $k_{\Delta} = 1.02$, respectively. In the design stage, the layer coefficient (k_{Δ}) and the nominal porosity (P) determine the placing density and the estimation of the total number of armor units required to armour the breakwater.

In the case of a HLCS, the layer thickness is a key parameter to calculate the crest elevation which determines the amount of wave energy transmission. In this study, a BPE numerical model is validated to measure the layer thicknesses and crest elevation of Cubipod HLCSs. Fig. 2 shows the front view and relative dimensions of the Cubipod units (three orthogonal planes of symmetry) modeled in Blender (2019).

3. Validation of the numerical model

3.1. Small-scale physical model placement tests

3D physical and numerical model placement tests were conducted to estimate the layer thicknesses of five-layer Cubipod HLCSs. When constructing a HLCS, rectangular and triangular placement grids can be considered (Odériz et al., 2018). The type of placement grid and its geometric parameters (Fig. 3) will determine the layer thickness and armor porosity. The geometric parameters of the placement grids are related to the nominal diameter of the units. Fig. 3a illustrates the rectangular placement grid (RPG) used in this study with separations of $a/D_n = 1.40$ and $b/D_n = 1.30$ along the X and Y directions, respectively, and Fig. 3b illustrates the triangular placement grid (TPG) with separations of $a/D_n = 1.58$ and $b/D_n = 1.27$. Wave direction corresponds to the Y-direction (Odériz et al., 2018).

The 3D physical model placement tests were conducted in the Laboratory of Ports and Coasts at the Universitat Politècnica de València on a horizontal rigid bottom (De Keyser and Jacobs, 2020). For each placement grid, the first layer of Cubipods was randomly oriented and placed by hand over a printed scheme of the unit centers of gravity; the Cubipods of the first layer always rested with a side on the flat rigid bottom (minimum potential energy). The following layers were randomly placed by hand on the hollows of the lower layer (minimum potential energy) following the conventional placement approach. A rigid structure with a mobile horizontal beam was placed on the physical model to measure distances to a reference horizontal plane. A laser measuring device was placed on the horizontal beam to measure the vertical distance from the plates placed on the top of each layer to the reference horizontal plane (Fig. 4 and Fig. 5a). Once each layer was placed, the layer coefficient, $k_{\Delta j}$, was calculated as

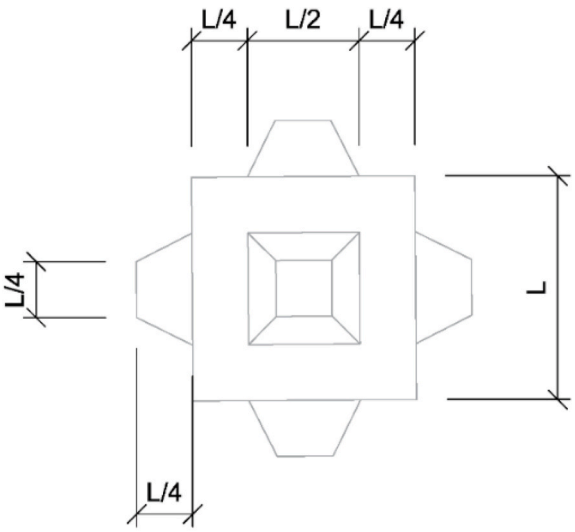

Fig. 2. Relative dimensions of a Cubipod unit.

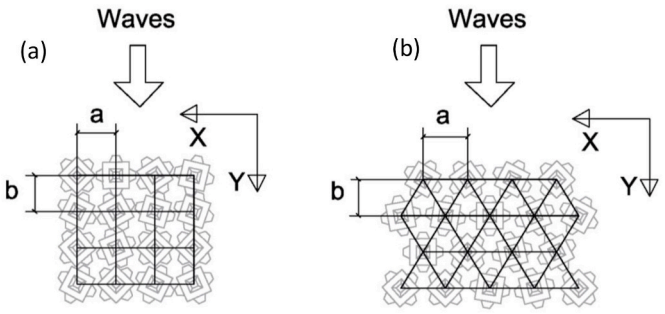

Fig. 3. Geometric parameters of the placement grids: (a) RPG and (b) TPG.

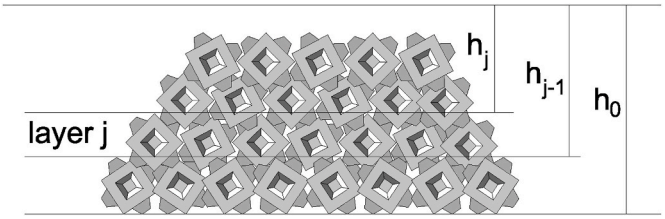

Fig. 4. Measurement of the layer thickness of layer j (Eq. (3)).

$$k_{\Delta j} = \frac{(h_{j-1} - h_j)}{D_n} \tag{3}$$

where the difference between the mean vertical distance from top of the armor units (Fig. 4) measured on the previous layer (h_{j-1}) and the actual one (h_j) is divided by the nominal diameter (D_n [cm] = 3.80 in this case). For the first layer (j = 1), h_0 was the distance between the horizontal and rigid bottom and a reference envelope plane on top of the armor units. Fig. 4 illustrates the evaluation of the layer coefficient with Eq. (3).

The measurement of the layer coefficient with this methodology is dependent on the area where the envelope is measured. In this study, squared plates of dimension $2D_n$x$2D_n$ were manufactured using a rigid material and were placed on top of the layers. The measurements of structure height were taken at the center of the squared plates (see Fig. 5b). Since several measurements of the structure height were obtained per each layer (j), the mean value was calculated (h_j). In order to assess the variability on the layer coefficient, five repeatability physical model placement tests of five-layer Cubipod HLCSs were conducted for both the RPG and TPG grids.

Fig. 5a shows the framework used to measure the layer thickness in the laboratory. Fig. 5b illustrates a detail of the squared plate with size $2D_n$x$2D_n$ used to measure the structure height with the laser device.

3.2. Numerical model placement tests

3.2.1. Mathematical model

Millington (2007) defined the mathematical model of any physics engine. The Bullet Physics Engine (BPE) is based on Newton's laws of motion:

$$\boldsymbol{F} = m \cdot \boldsymbol{a} \tag{4}$$

$$\boldsymbol{M} = I \cdot \boldsymbol{\alpha} \tag{5}$$

where the three-component vector **F** is the resultant of all the forces acting on the object, the 3 × 3 (diagonal) matrix m is the mass of the object, **a** is the linear acceleration, the three-component vector **M** is the resultant of all the moments acting on the object, the 3 × 3 (symmetric) matrix I is the inertia of the object and **α** is the angular acceleration. Given a set of forces and moments acting on the object, BPE integrates twice the linear and angular accelerations to obtain the position and orientation of the object. BPE calculates the position on each time step until the object is in the final position without any movement.

In order to decrease the computational time, Eqs. (4) and (5) are numerically solved using the Euler's Method. Indeed, some inaccuracy is considered acceptable in the simulation to make feasible the numerical analysis. Euler's Method evaluates the velocity at a time interval t and predicts the next velocity at t+Δt assuming a constant velocity during Δt. The smaller the Δt, the better the accuracy, but the higher the computational time. BPE considers a non-physical reduction on the linear and angular velocities at each time step using damping factors in order to obtain realistic and stable simulations. The estimation of the linear and angular velocities at each time step can then be expressed as follows:

$$\dot{\boldsymbol{s}}_{i+1} = \dot{\boldsymbol{s}}_i - \dot{\boldsymbol{s}}_i d + \ddot{\boldsymbol{s}}_i t \tag{6}$$

$$\dot{\boldsymbol{\theta}}_{i+1} = \dot{\boldsymbol{\theta}}_i - \dot{\boldsymbol{\theta}}_i(d_a) + \ddot{\boldsymbol{\theta}}_i t \tag{7}$$

where d and d_a are linear and angular damping parameters, respectively, $\dot{\boldsymbol{s}}_{i+1}$ and $\dot{\boldsymbol{\theta}}_{i+1}$ are the linear and angular velocities of the object at t= (i+1)Δt = t_{i+1}, $\dot{\boldsymbol{s}}_i$ and $\dot{\boldsymbol{\theta}}_i$ are the linear and angular velocities of the object at t = iΔt = t_i, $\ddot{\boldsymbol{s}}_i$ and $\ddot{\boldsymbol{\theta}}_i$ are the linear and angular accelerations of the object at t = t_i, and Δt is the time step.

When the simulation has more than one object, they can collide with each other. To solve the collision problem, Izadi and Bejuizen (2018) explain that DEMs use the soft contact models proposed by Cundall (2001) while Physics Engines use the hard contact models proposed by Moreau (1999) and Jean (1999). On the one hand, soft contact models accurately solve the collision in small increments of discrete time so they provide the variation of velocity during the collision. On the other hand, hard contact models are not interested in the collision itself but only in the post-collision velocities of the objects which are estimated as a result of momentum exchange; therefore, hard contact models do not

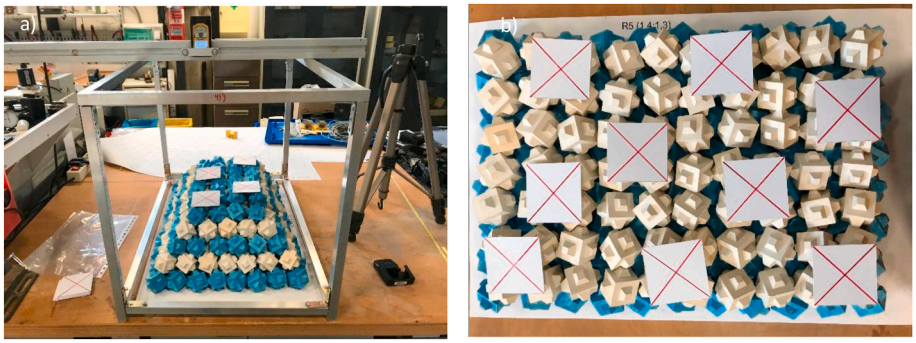

Fig. 5. Physical model placement tests: (a) general view and (b) detail of the plates used to measure layer thickness.

explicitly solve the collision. The time interval used for hard contact models can be much higher than those for soft contact models, decreasing the computing time, especially when a large number of elements has to be modeled.

BPE uses a hard contact model with a relatively large time-stepping scheme to solve rigid body collisions. In that model, a collision-detection procedure identifies the colliding objects. The velocities post-collision are then calculated based on the pre-collision velocities. Finally, the velocities, positions and orientations of the rigid bodies are updated based on Eqs. (4) and (5). The fundamentals of hard contact models are discussed below. For further details, readers are referred to Izadi and Bejuizen (2018) and Radjai and Richefeu (2009).

The collision of two objects can be modeled with normal and tangential contact velocities, $\dot{s}_n$and $\dot{s}_t$, respectively, and normal and tangential contact forces, $f_n$and $f_t(=\mu f_n)$, respectively, where μ is the friction coefficient. Hard contact models split the contact velocities into the velocities at $t = t_i$ and $t = t_{i+1}$, therefore the contact velocities are rewritten as

$$\dot{s}_n = \frac{\dot{s}_{n,i+1} + e_n \dot{s}_{n,i}}{1 + e_n} \tag{8}$$

$$\dot{s}_t = \frac{\dot{s}_{t,i+1} + e_t \dot{s}_{t,i}}{1 + e_t} \tag{9}$$

where e_n and e_t are the normal and tangential parts of the restitution coefficients, $\dot{s}_{n,i}$and $\dot{s}_{n,i+1}$ are the normal contact velocities at $t = t_i$ and t_{i+1}, respectively, and $\dot{s}_{t,i}$and $\dot{s}_{t,i+1}$ are the tangential contact velocities at $t = t_i$ and t_{i+1}, respectively. The hard contact method allows writing the equations of motion of each object considering the velocities given by Eqs. (8) and (9) in the Newton's laws of motion given by Eqs. (4) and (5).

3.2.2. Parameters that affect the Bullet Physics Engine (BPE) simulations

The physics fundamentals of the numerical approximation used by BPE are described in Section 3.2.1. which pointed out the existence of some parameters which may influence the numerical simulation. The reliability of the numerical simulation will depend on the adequate selection of the five parameters listed below.

(1) **Friction (μ)**: It is the relationship between normal and tangential forces. In BPE model, it represents a mean value between static and dynamic friction coefficients. The friction coefficient mainly depends on the unit material; for concrete commonly used for armor units, it is usually in the range $0.5 < \mu < 1.0$. The higher the friction factor, the higher the tangential force between objects.
(2) **Bounciness (e)**: It is related to the restitution coefficient of the object. Considering two objects after a collision, it is the ratio of the final to the initial relative velocity. Bounciness is in the range $0 \leq e \leq 1$, where a value $e = 0$ indicates a fully inelastic collision and a value $e = 1$ indicates a fully elastic collision.
(3) **Linear Damping (d)**: It is a numerical parameter in the range $0 \leq d \leq 1$ included in Eq. (6) to obtain realistic and stable simulations reducing the amount of linear velocity at each time step. The higher the linear damping factor, the higher the reduction in the linear velocities of the objects.
(4) **Angular Damping (d_a)**: It is a numerical parameter in the range $0 \leq d_a \leq 1$ included in Eq. (7) to obtain realistic and stable simulations reducing the amount of angular velocity at each time step. The higher the angular damping factor, the higher the reduction in the angular velocities of the objects.
(5) **Collision Margin (CM)**: It is the threshold of distance where collisions are still considered. It is used to improve the stability of rigid-bodies during the numerical simulation; a collision margin gives the BPE a margin of error in detecting and resolving contacts. The lower the Collision Margin, the closer the collisions are detected and the more realistic is the response.

3.2.3. Numerical model placement tests of cubipod HLCSs

Physical model placement tests were carried out using small-scale Cubipods units with a nominal diameter D_n [cm] = 3.80. The corresponding numerical model placement tests were conducted at prototype scale with D_n [m] = 1.07, corresponding to a Cubipod with side L [m] = 1.00, because instabilities were observed with small units due to numerical precision. Fig. 2 shows the front view and dimensions of the Cubipod units modeled in Blender (2019). The mass of those Cubipods was considered to be W [t] = $2.3 \times Dn^3$ corresponding to typical unreinforced concrete units. The simulations were conducted with $e = d = d_a = 0$, $\mu = 0.6$, D_n [m] = 1.07 and $CM/D_n = 0.008$. Falling distance (FD) was $FD/D_n = 0.25$ and gravity acceleration was set to g [m/s^2] = 9.81. FD was measured from the total height of the previous layers considering the layer coefficient of each layer.

Each layer of Cubipods was placed according to a placement grid. To follow the hand placement of the physical model tests in the numerical model, the placement grid of each layer was referred to a single Cubipod unit placed on the lower layer (namely "layer reference"), and all units of the layer were dropped under the gravity acceleration from the falling distance (FD). All the armor units of each layer were dropped at the same time; once the unit movements ceased, the units of this layer were fixed and those armor units did not interact as moving rigid bodies with the next layers.

Fig. 6a and b illustrate the placement of the second layer of Cubipod units before and after dropping the elements with RPG (a/Dn = 1.40 and b/Dn = 1.30). Fig. 7a and b shows the front view and side view of a five-layer Cubipod HLCS model with RPG (a/Dn = 1.40 and b/Dn = 1.30).

The placement of the $2D_n \times 2D_n$ squared plates used to measure the height of the structure in the physical model tests was reproduced in the numerical model. The plates were dropped and the distances between the horizontal rigid bottom and the centers of the squared plates were measured. Fig. 8a and b illustrate the squared plate placement corresponding to the third and fourth layers. At least six measurements were taken in each layer to calculate the mean value of the height of the structure to estimate the corresponding layer coefficients given by Eq. (2). In order to assess the variability on the layer coefficient, five repeatability numerical model placement tests corresponding to five-layer Cubipod HLCSs were conducted for both the RPG and TPG grids. The armor units of the first layer were randomly oriented with one edge on the flat rigid bottom while the second to fifth layers were placed on the previous one with random orientation. Two videos are available to see the performance of the numerical simulations with TPG and RPG.

3.2.4. Sensitivity analysis

The sensitivity of the simulations to the physical and numerical parameters described in Section 3.2.2 (μ, e, d, d_a and CM) as well as the falling distance (FD) is analyzed here. To this end, 250 Cubipods were used to build up a numerical three-layer Cubipod HLCS using BPE; the corresponding layer coefficients were calculated following the methodology defined in section 3.2.3 with a RPG grid. The numerical simulations were conducted with parameters given in Table 1.

For each layer, the relative error between the physical and numerical model tests was estimated as

$$\varepsilon r_j = \frac{\left| k_{\Delta jP} - k_{\Delta jN} \right|}{k_{\Delta jP}} \tag{10}$$

where $k_{\Delta jN}$ is the estimated layer coefficient in the numerical model tests and $k_{\Delta jP}$ is the measured layer coefficient in the physical model tests. The global mean relative error of the layer coefficients was evaluated as

$$\varepsilon_R = \frac{\sum_{j=1}^{M} \varepsilon r_j}{M} \tag{11}$$

where εr_j is the relative error of the jth layer and M is the number of layers of the model. In this case, M = 3 and $1.9 < \varepsilon_R$ (%) < 7.6; the BPE was found to be a robust software with low sensitivity to the values of

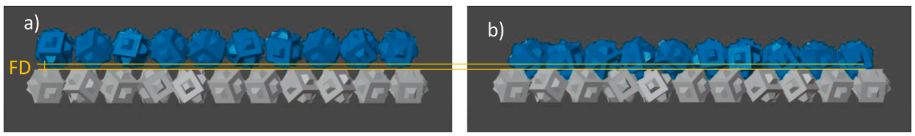

Fig. 6. Placement of the second layer of units in a two-layer Cubipod HLCS using RPG (a/Dn = 1.40 and b/Dn = 1.30): (a) before the second layer placement and (b) after the econd layer placement.

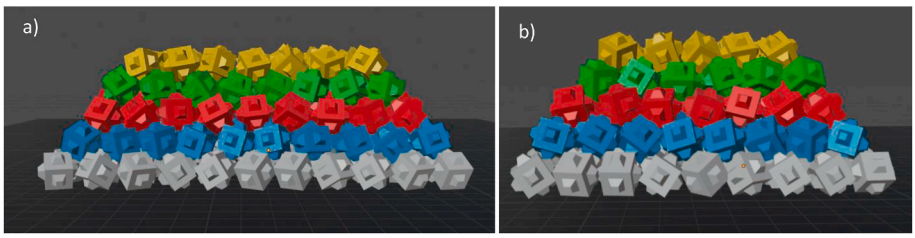

Fig. 7. Five-layer Cubipod HLCS using RPG with a/Dn = 1.40 and b/Dn = 1.30: (a) front view and b) side view.

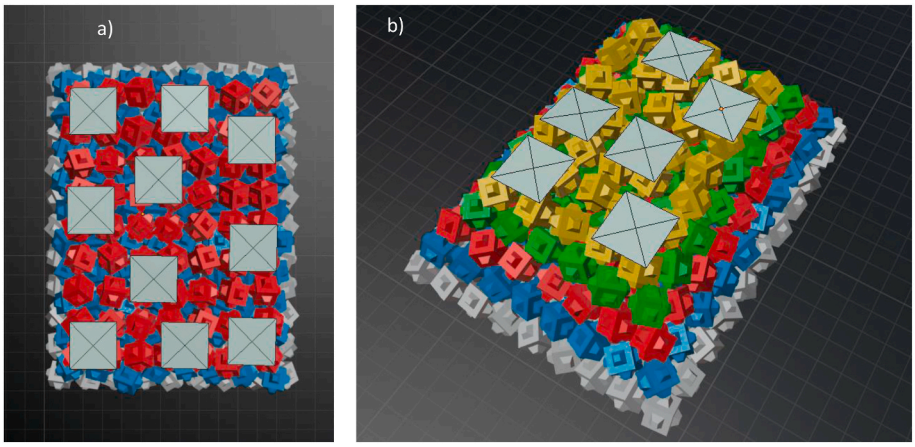

Fig. 8. Numerical placement of squared plates to measure the structure height: (a) top view of the third layer and (b) general view of the fourth layer.

Table 1
Parameters used in the numerical simulations.

Parameter	Value
μ	0.6, 0.7, 0.8
e	0.00, 0.05, 0.10
d	0.0, 0.5, 1.0
d_a	0.0, 0.5, 1.0
CM/D_n	0.008, 0.010, 0.012
FD/D_n	0.10, 0.15, 0.20, 0.25, 0.30, 0.35, 0.40
L [m] (D_n [m])	0.5 (0.53), 1.0 (1.07), 1.5 (2.14)

the physical and numerical parameters (μ, e, d, d_a, CM, FD and D_n) used to measure the layer coefficient of Cubipod HLCSs. The parameters which showed the lowest ε_R were μ = 0.6, e = 0, d = 0, da = 0, CM/D_n = 0.008, FD/D_n = 0.25 and D_n [m] = 1.07 which corresponds to L [m] = 1.0.

3.3. Calibration

Table 2 shows the mean value $\overline{k_{\Delta j}}$ and the coefficient of variation $CV(k_{\Delta j})$ of the layer coefficients (1≤ j ≤ 5) measured in physical (De Keyser and Jacobs, 2020) and numerical (Centi, 2020, and this study) model placement tests. $\overline{k_{\Delta j}}$ were similar for physical and numerical model tests while $CV(k_{\Delta j})$ were slightly higher for the physical model placement tests and also in numerical model tests conducted by Centi (2020) when compared to the tests conducted in this study. Here, the BPE parameters (μ, e, d, d_a, CM, FD, and D_n) were selected after the sensitivity analysis described above, while the parameters used by Centi (2020) were not optimized. The numerical model tests conducted in this study showed a low global mean relative error: ƐR (%) (RPG) = 1.39 and ƐR (%) (TPG) = 1.04 (Table 2). Five-layer Cubipod HLCSs placed using RPG (a/Dn = 1.4 and b/Dn = 1.3) showed a total height of the structure lower than that using TPG (a/Dn = 1.58 and b/Dn = 1.27). The dimensionless placing densities were ϕ = 0.55 and 0.50 for RPG and TPG, respectively. The mean value of the layer coefficient measured in the physical model placement tests was satisfactorily estimated with the BPE numerical simulations.

The first layer, j = 1, is influenced by the horizontal rigid bottom, providing a much higher layer coefficient compared to layers placed on a previously placed layer of Cubipods. The second layer, j = 2, is indirectly influenced by the horizontal rigid bottom and showed a significantly higher layer coefficient compared to the upper layers. The third layer and upper layers of Cubipods have a similar layer coefficient.

Fig. 9 illustrates the 95% confidence interval of the layer coefficients ($k_{\Delta j}$) measured in the physical and numerical model placement tests analyzed in this study. The 95% confidence intervals are estimated as

$$\overline{k_{\Delta j}} \Big/ \sqrt{N}\left[1 \pm 1.96 CV\left(k_{\Delta j}\right)\right] (1 \leq \cdot j \cdot \leq 5) \tag{12}$$

where N is the number of tests, $\overline{k_{\Delta j}}$ is the mean value and CV($k_{\Delta j}$) is the

Table 2
Physical and numerical measurements of the layer coefficients of Cubipod HLCSs corresponding to RPG ($a/D_n = 1.4$ and $b/D_n = 1.3$) and TPG ($a/D_n = 1.58$ and $b/D_n = 1.27$) on horizontal rigid bottom.

		Horizontal rigid bottom								
		Physical model placement tests ($k\Delta j$)		Numerical model placement tests from this study ($k\Delta j$)		Numerical model placement tests from Centi (2020) ($k\Delta j$)		εr_j (%) from this study Eq. (10)	εr_j (%) from Centi (2020) Eq. (10)	ε_R (%) from this study Eq. (11)
		$\overline{k_{\Delta j}}$	$CV(k_{\Delta j})$	$\overline{k_{\Delta j}}$	$CV(k_{\Delta j})$	$\overline{k_{\Delta j}}$	$CV(k_{\Delta j})$			
RPG	L1	1.319	0.005	1.319	0.000	1.321	0.012	0.01	0.14	1.39
	L2	1.052	0.014	1.081	0.007	1.086	0.049	2.79	3.20	
	L3	0.939	0.019	0.960	0.005	0.931	0.123	2.24	0.87	
	L4	0.949	0.018	0.935	0.013	0.943	0.143	1.47	0.64	
	L5	0.915	0.040	0.919	0.019	0.906	0.112	0.45	0.94	
TPG	L1	1.294	0.008	1.317	0.000	1.312	0.009	1.83	1.39	1.04
	L2	1.076	0.008	1.079	0.012	1.125	0.043	0.32	4.51	
	L3	0.980	0.016	0.980	0.016	1.001	0.082	0.03	2.18	
	L4	0.970	0.022	0.983	0.011	1.024	0.125	1.32	5.53	
	L5	0.984	0.020	0.968	0.022	0.991	0.082	1.68	0.72	

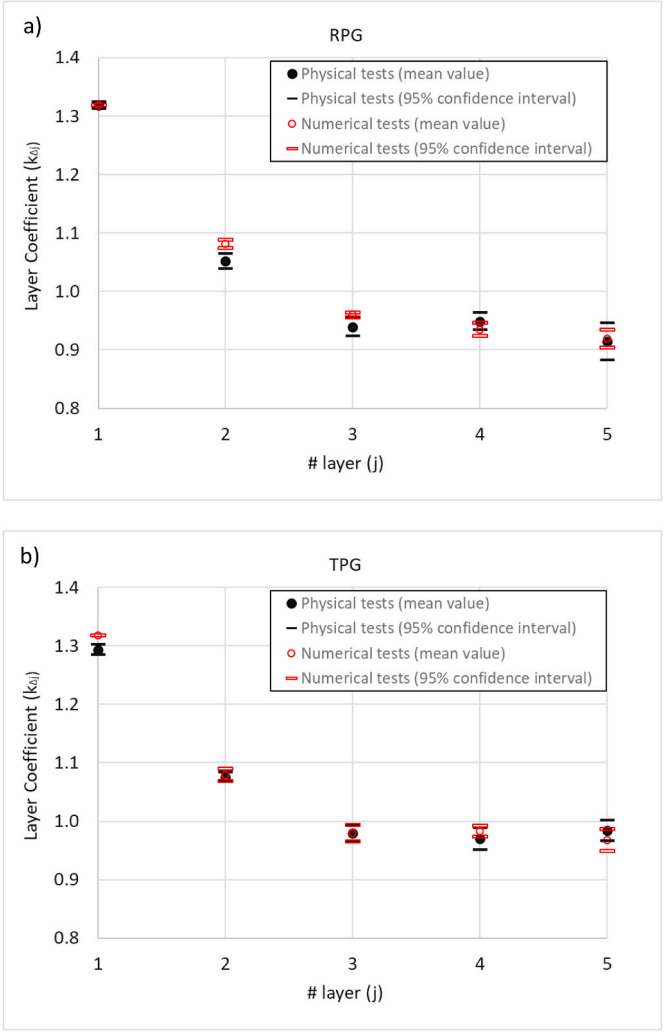

Fig. 9. Layer coefficient ($k_{\Delta j}$) as a function of the layer number (j). Mean values and 95% confidence intervals for physical and numerical model placement tests using (a) RPG (ϕ= 0.55) and (b) TPG (ϕ= 0.50) on a horizontal rigid bottom.

coefficient of variation which depends on the layer number (j). The 95% confidence intervals for $k_{\Delta j}$ overlap for physical and numerical model tests for most of the tested cases. It can be concluded that any difference in the measurements of $k_{\Delta j}$ is well explained by the measurement error described by $CV(k_{\Delta j})$; BPE may be considered a suitable tool to estimate the layer coefficients of Cubipod HLCSs placed on horizontal rigid bottoms.

De Keyser and Jacobs (2020) noted that the layer coefficient of the first layer of Cubipod units, placed on a horizontal rigid bottom, can be calculated theoretically from the geometry of the Cubipod units (see Fig. 2) as $k_{\Delta 1} = 1.298$ (position with the lowest center of gravity). Considering both physical and numerical model placement tests conducted in this study (see Table 2), a reasonable estimation of the mean layer coefficient of a Cubipod HLCS on horizontal rigid bottom is given by

$$k_{\Delta 1} = 1.30 \tag{13a}$$

$$k_{\Delta 2}(\text{RPG}) = 1.07 \text{ and } k_{\Delta 2}(\text{TPG}) = 1.10 \tag{13b}$$

$$k_{\Delta j}(\text{RPG}) = 0.93 \text{ and } k_{\Delta j}(\text{TPG}) = 0.99;\ 3 \leq j \leq 5 \tag{13c}$$

In which RPG refers to a rectangular placement grid with $\phi = 0.55$ ($a/Dn = 1.4$ and $b/Dn = 1.3$) and TPG refers to a triangular placement grid with $\phi = 0.50$ ($a/Dn = 1.57$ and $b/Dn = 1.28$). The height of a n-layer Cubipod HLCS on a horizontal rigid bottom slope (H) can be estimated using Eq. (14) with the layer coefficients defined in Eqs. (13), considering the height as the distance between the upper and lowest plane envelopes of the HLCS.

$$H = \sum_{j=1}^{j=N} k_{\Delta j} D_n \tag{14}$$

4. Validation and application

Once the BPE numerical model was calibrated using results from physical model placement tests on horizontal rigid bottom, nine additional realistic five-layer Cubipod HLCS models were constructed in the wave flume at the Universitat Politècnica de València (30 × 1.2 × 1.2 m). The new Cubipod HLCS physical models were placed by hand following a TPG with $\phi = 0.50$ ($a/D_n = 1.58$ and $b/D_n = 1.27$) on a 4% rigid bottom slope. Fig. 10a shows the side view of the five-layer Cubipod HLCS. The layer coefficient was measured with a method similar to that described in section 3.1. The measurements were taken at a fixed distance from the wave paddle and at three different locations along the HLCS model.

The BPE was used to simulate the construction of Cubipod HLCSs on the wave flume. In order to somehow emulate the physical hand placement, a "layer reference" was assumed: the placement grids of the second to the fifth layer were referred to the measured position of one of the Cubipod units placed in the lower layer. Thus, the placement grid of each layer is somehow dependent on the final positions of the Cubipod

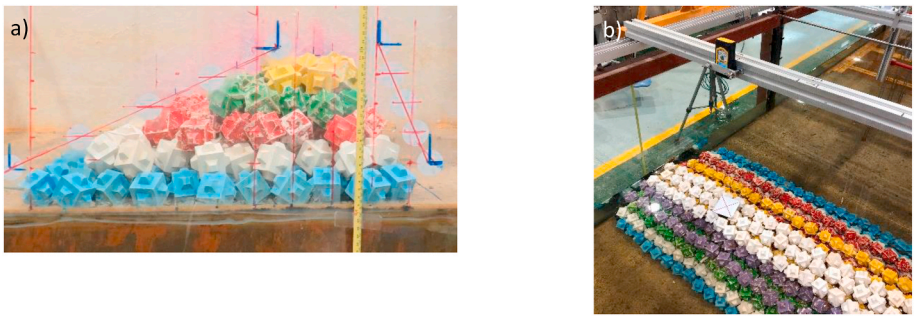

Fig. 10. Five-layer Cubipod HLCS model placed in the wave flume: (a) side view and (b) measuring system to estimate the layer coefficients.

units in the lower layers. The units of the first layer were randomly oriented with an edge on the bottom following the TPG ($a/D_n = 1.58$ and $b/D_n = 1.27$) on a 4% rigid bottom slope, while the units of the second to the fifth layer were placed on the previous layer with random orientation. Five numerical model tests were conducted using BPE with the TPG described above and the parameters which showed the lowest ε_R given in section 3.2. The layer thickness was measured on 12 areas in the first layer, 9 areas in the second and third layer, 6 areas in the fourth layer and 3 areas in the fifth layer. Fig. 11a and b shows the side and top views of the five-layer Cubipod HLCS numerical model. Each test took approximately 20 min on a conventional PC using 24 frames per second.

Table 3 shows the mean value $\overline{k_{\Delta j}}$ and the coefficient of variation $CV(k_{\Delta j})$ of the layer coefficients ($1 \leq j \leq 5$) measured in physical and numerical model placement tests. $\overline{k_{\Delta j}}$ were similar for physical and numerical model tests while $CV(k_{\Delta j})$ were slightly higher for the physical model placement tests.

Fig. 12 compares the layer coefficients measured in the physical and numerical model tests (mean value and 95% confidence interval). Fig. 12 illustrates that the BPE and physical model tests showed similar results. The numerical model tests conducted in this study on a 4% bottom slope showed a global mean relative error $\mathcal{E}_R$ (%) = 2.75 in the estimation of the layer coefficients, higher than $\mathcal{E}_R$ (%) = 1.04 given in Table 2 but good for practical applications.

Construction at prototype scale in real conditions is usually affected by poor underwater visibility which compel crane operators to strictly follow the prescribed placement grid. The BPE can be used to study conditions similar to the blind placement of a Cubipod HLCS to assess the workability of a given placement grid in these unfavorable but frequent conditions. To this end, a simulation with "blind reference" was conducted by referring the placement grids of all the layers to only a single Cubipod unit to be placed in the first layer. Fig. 13 illustrates the placement grids of three layers with "blind reference".

Fig. 14a shows the side view of the five-layer Cubipod HLCS placed with BPE using TPG (a/Dn = 1.58 and b/Dn = 1.27) and "blind reference"; the result is clearly worse (misplacement of some units) than that obtained using BPE with "layer reference". Fig. 14b shows that some Cubipod units fall out of the structure; the TPG (a/Dn = 1.58 and b/Dn = 1.27) is adequate in laboratory (construction by hand) and also at prototype scale with good visibility, but it may be challenging to construct such HLCS if the underwater visibility is poor. The BPE can be used to analyze the feasibility and quality of placement grids similar to those used in the laboratory to construct reliable Cubipod HLCSs in cases with good or poor underwater visibility.

Table 3
Physical and numerical measurements of the layer coefficients corresponding to TPG ($a/D_n = 1.58$ and $b/D_n = 1.27$) on a 4% rigid bottom slope with "layer reference" placement.

		4% rigid bottom slope					
		Physical model placement tests (kΔj)		Numerical model placement tests (kΔj)		εr_j (%) Eq. (10)	ε_R (%) Eq. (11)
		$\overline{k_{\Delta j}}$	$CV(k_{\Delta j})$	$\overline{k_{\Delta j}}$	$CV(k_{\Delta j})$		
TPG	L1	1.316	0.018	1.329	0.001	0.99	2.75
	L2	1.022	0.042	1.083	0.021	5.99	
	L3	0.967	0.047	0.981	0.030	1.47	
	L4	0.961	0.050	0.977	0.030	1.58	
	L5	0.946	0.046	0.982	0.039	3.74	

5. Discussion

At prototype scale, an uneven bathymetry can be mapped using echo sounders to be considered in the BPE numerical simulations. Thus, BPE simulations can be used to analyze the performance of different placement grids over the singularities of the bathymetry at the construction site and to select the most adequate placement grid. A HLCS for coral reef recovery will usually be placed on a hard sea bottom with insignificant settlement; however, if HLCSs were placed on sandy seabeds without a rock foundation, relevant scour and settlement would likely occur and the results of this study would not be directly applicable.

The performance of BPE simulations for simple armor unit geometries and random placement may be similar to Cubipod HLCSs analyzed in this study. Further research is necessary to evaluate the performance of BPE simulations using complex armor unit geometries or special placement techniques for interlocking.

The packing density of precast concrete armor units critically

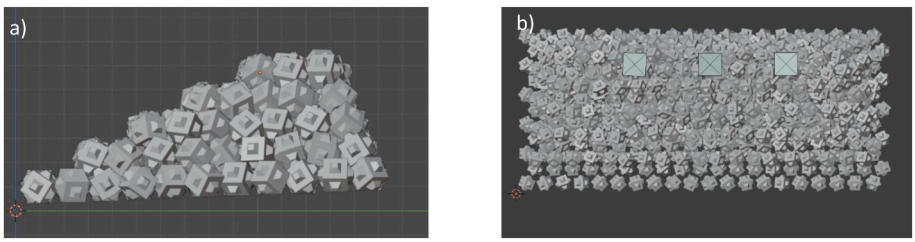

Fig. 11. Five-layer Cubipod HLCS constructed with BPE following a TPG (a/Dn = 1.58 and b/Dn = 1.27) with "layer reference": (a) side view, and (b) top view with three squared plates placed on the fifth layer.

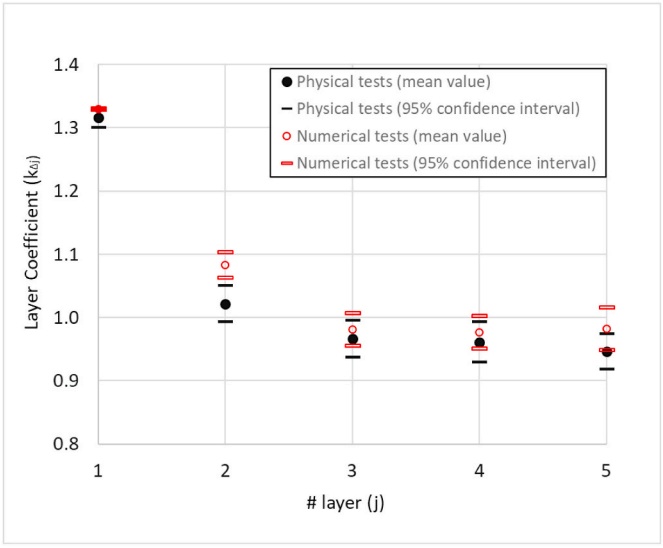

Fig. 12. Mean values and 95% confidence intervals of layer coefficient ($k_{\Delta j}$) as a function of the layer number (j) corresponding to TPG (ϕ= 0.50) on a 4% rigid bottom slope with "layer reference" placement.

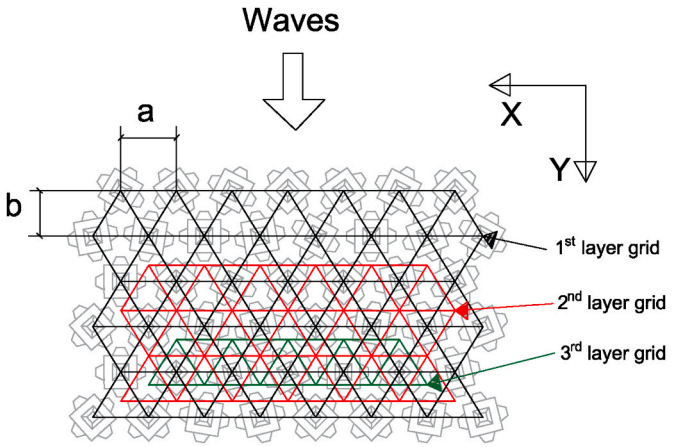

Fig. 13. Triangular placement grid (TPG) used in BPE to simulate the blind placement: first layer (black), second layer (red), and third layer (green).

depends on the placement grid and packing density affects the cost and logistics of the breakwater construction and also the breakwater performance (armor hydraulic stability, overtopping, etc.). BPE simulations can be used to test different placement grids in order to select the one which provides the optimum packing density on the trunk, the roundhead and other sections of the breakwater. Moreover, mound breakwaters are frequently damaged by storms and BPE may be a suitable tool to assess the workability of a given repair strategy; the damaged breakwater can be mapped with echo sounders and different units and placement grids can be considered to choose the best feasible repair process.

6. Summary and conclusions

This study analyzes the feasibility of the numerical model Bullet Physics Engine (BPE) in representing the construction of Cubipod HLCSs in order to estimate the HLCS height and layer coefficients. The BPE numerical model is calibrated and validated with physical model placement tests of five-layer Cubipod HLCSs on 0% and 4% flat rigid bottom slopes. The layer coefficients are measured for specific rectangular and triangular placement grids considered for small-scale hydraulic stability testing focusing the experimental effort in the triangular placement grid TPG with ϕ = 0.50 (a/Dn = 1.58 and b/Dn = 1.27) proposed by Odériz et al. (2018) for Cubipod HLCSs.

BPE numerical model showed a very low sensitivity to the physical and numerical parameters; good results were found using: $\mu = 0.6$, $e = d = d_a = 0$, $CM/D_n = 0.008$, $FD/D_n = 0.25$, and D_n [m] = 1.07 (L [m] = 1.00). BPE using a TPG (a/Dn = 1.58 and b/Dn = 1.27) with "layer reference", somehow emulating hand placement, showed a global mean relative error of ε_R (%) (TPG) = 1.04 when compared to the measurements taken in small-scale physical model tests of five-layer Cubipod HLCSs placed on a horizontal rigid bottom. The mean value of the layer coefficients, $\overline{k_{\Delta j}}$, measured in both physical and numerical models were similar, and the coefficient of variation, CV($k_{\Delta j}$), were slightly higher for the physical model tests. As expected, layer coefficients and structure height of Cubipod HLCSs depend on the placement grid; for each type of placement grid, the lower the placing density, the lower the layer thickness and structure height, except the layer coefficient of the first layer which is related to the unit geometry and characteristics of the bottom ($k_{\Delta 1} = 1.30$ for Cubipod units on flat rigid bottom).

BPE using a TPG (a/Dn = 1.58 and b/Dn = 1.27) with "layer reference", emulating hand placement, showed a global mean relative error of ε_R (%) = 2.75 when compared to the measurements taken in small-scale physical model tests of a five-layer Cubipod HLCS placed on 4% rigid bottom slope. BPE also indicates that several units were incorrectly placed when using "blind reference", emulating placement with poor underwater vision, contrary to no unit lost when using "layer reference", somehow emulating placement with good underwater vision. The BPE numerical model was found to be a suitable tool to study the workability of placement grids of Cubipod HLCSs in realistic conditions.

The total height of HLCSs affects crest freeboard, wave transmission and the functionality of the structure. Crest freeboard is relatively easy to control and measure in laboratory tests whereas it is very difficult to control and measure at prototype scale. Small-scale physical models are usually placed by hand with a perfect vision, while prototypes are usually constructed using cranes with poor underwater vision. Changing only the "layer reference" by "blind reference", BPE simulations have shown significant differences in the workability of the same placement grid. The quality of the underwater vision during construction affects the most adequate placement grid to be used and BPE is a valuable tool to find the best placement grid for the prescribed construction conditions.

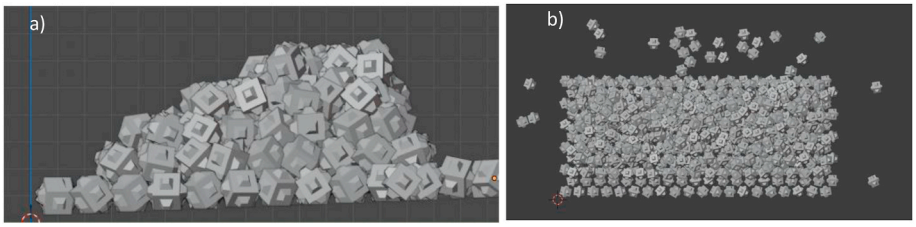

Fig. 14. Five-layer Cubipod HLCS constructed with the BPE following a TPG (a/Dn = 1.58 and b/Dn = 1.27) with "blind reference": (a) lateral view, and (b) top view.

CRediT authorship contribution statement

Jorge Molines: Conceptualization, Methodology, Software, Validation, Formal analysis, Resources, Writing – original draft, Writing – review & editing, Visualization, Supervision. **Riccardo Centi:** Methodology, Software, Validation, Formal analysis, Writing – review & editing. **Marcello Di Risio:** Methodology, Formal analysis, Visualization, Validation, Writing – review & editing. **Josep R. Medina:** Conceptualization, Methodology, Validation, Formal analysis, Resources, Writing – review & editing, Funding acquisition.

Declaration of competing interest

The authors declare that they have no known competing financial interests or personal relationships that could have appeared to influence the work reported in this paper.

Acknowledgements

The authors thank the two anonymous reviewers for their constructive comments and suggestions, the financial support of the Spanish Ministerio de Ciencia, Innovación y Universidades (Grant RTI 2018-101073-B-I00) and also Karel De Keyser and Elias Jacobs for conducting the physical placement test.

Appendix A. Supplementary data

Supplementary data to this article can be found online at https://doi.org/10.1016/j.coastaleng.2021.103901.

Nomenclature

List of symbols

a	placement grid separation in the X axis
$\mathbf{a}$	linear acceleration
b	placement grid separation in the Y axis
d_a	angular damping
d	linear damping
D_n	nominal diameter
e	bounciness
$\mathbf{f_n}$	normal contact forces
$\mathbf{f_t}$	tangential contact forces
$\mathbf{F}$	resultant of all forces acting on an object
g	gravity acceleration
h_j	mean vertical distance measured from the measurement device to the tope of layer j
I	intertia
k_Δ	layer coefficient
$\overline{k_{\Delta j}}$	mean value of the layer coefficient of layer j using all the laboratory measurements of the layer
L:	length of the Cubipod edge
m	mass
$\mathbf{M}$	resultant of all moments acting on an object
M	number of layers in a HLCS
n	number of layers to estimate the placing density in conventional mount breakwaters
N	number of tests to estimate the confidence interval of $\overline{k_{\Delta j}}$
P	nominal Porosity
$\mathbf{s}, \dot{\mathbf{s}}, \ddot{\mathbf{s}}$	linear position, velocity, acceleration
W	weight
$\boldsymbol{\alpha}$	angular acceleration
$\mathcal{E}_R$	global mean relative error
$\mathcal{E}r$	relative error
φ	placing density
ϕ	packing density
Υ	specific weight
μ	friction factor
ρ	mass density
$\boldsymbol{\theta}, \dot{\boldsymbol{\theta}}, \ddot{\boldsymbol{\theta}}$	angular position, velocity, acceleration

Subscripts

j	layer number

Acronyms

BPE	Bullet Physics Engine
CFD	Computational Fluid Dynamics
CM	Collision Margin
CV	Coefficient of Variation

DEM	Discrete Element Method
FD	Falling Distance
FEM	Finite Element Method
HLCS	Homogeneous Low-Crested Structure
LCS	Low-Crested Structure
RPG	Rectangular Placement Grid
TPG	Triangular Placement Grid

References

Anastasaki, E., Latham, J.P., Xiang, J., 2015. Numerical modelling of armor layers with reference to Core-Loc units and their placement acceptance criteria. Ocean. Eng. 104, 204–218.

Blender, 2019. Blender 2.80 Reference Manual. Available at: https://www.blender.org/and visited in January 2020.

Centi, R., 2020. Placement of Homogeneous Artificial Mound Breakwaters Using a Game Engine. MSc. Thesis, University of L'Aquila (ITA). October 2020, 80.

Ciria, C.U.R., CETMEF, 2007. The Rock Manual: the Use of Rock in Hydraulic Engineering, second ed. CIRIA, London, p. C683.

Cooper, A.K., Greben, J.M., van den Bergh, F., Gledhill, I., Canoo, B., Steyn, W.J., de Villiers, R., 2008. A Preliminary Physics-Engine Model of Dolosse Interacting with One Another. Sixth South African Conference on Computational and Applied Mechanics, SACAM08, Pretoria (South Africa), pp. 26–28. March.

Cooper, A.K., de Villiers, R., Greben, J.M., van den Bergh, F., Gledhill, M.A., 2010. Simulating the Rubble Mound Underlying Armor Units Protecting a Breakwater. Seventh South African Conference on Computational and Applied Mechanics. SACAM10, Pretoria (South Africa), 10-13 January.

Cundall, P.A., 2001. A discontinuous future for numerical modelling in geomechanics. Proc. Inst. Civ. Eng. Geotech. Eng. 149 (1), 41–47.

De Keyser, K., Jacobs, E., 2020. Literature Review on Low-Crested and Submerged Structures. MSc. Thesis, Ghent University (BE), p. 116. June 2020.

Dupray, S., Roberts, J., 2009. Review of the Use of Concrete in the Manufacture of Concrete Armor Units. Proceedings Int. Conf. of Coasts, Marine Structures and Breakwaters. Institution of Civil Engineers (ICE), London (UK), 16-18 September.

Ferrario, F., Beck, M.W., Storlazzi, C.D., Micheli, F., Shepard, C.C., Airoldi, L., 2014. The effectiveness of coral reefs for coastal hazard risk reduction and adaptation. Nat. Commun. 5 (3794), 98–101.

Frens, A.B., 2007. The Impact of Placement Method on Antifer-Block Stability. MSc. Thesis, Delft Univ. of Technology (NET), p. 146. May 2007.

Greben, J.M., Cooper, A.K., Gledhill, I., de Villiers, R., 2008. Numerical Modelling of Structures of Dolosse and Their Interaction with Waves. 2nd CSIR Biennial Conference, Pretoria (South Africa), 17-18 November.

Greben, J.M., Gledhill, I., Cooper, A.K., de Villiers, R., 2010. Characterization and Properties of Breakwater Structures Modelled by a Physics Engine. Seventh South African Conference on Computational and Applied Mechanics, SACAM10, Pretoria (South Africa), 10-13 January.

Guo, L., Latham, J.P., Xiang, J., 2015. Numerical simulation of breakages of concrete armor units using a three-dimensional fracture model in the context of the combined finite-discrete element method. Comput. Struct. 117–142.

Izadi, E., Bejuizen, A., 2018. Simulating direct shear tests with the Bullet physics library: a validation study. PloS One 13 (4), e0195073. https://doi.org/10.1371/journal.pone.0195073.

Jean, M., 1999. The non-smooth contact dynamics method. Comput. Methods Appl. Mech. Eng. 177 (3–4), 235–257.

Latham, J.P., Munjiza, A., Mindel, J., Xiang, J., Guises, R., Garcia, X., Pain, C., Gorman, G., Piggott, M., 2008. Modelling of massive particulates for breakwater engineering using coupled FEMDEM and CFD. Particuology 6, 572–583.

Latham, J.P., Anastasaki, E., Xiang, J., 2013. New modelling and analysis methods for concrete armor unit systems using FEMDEM. Coast Eng. 77, 151–166.

Medina, J.R., Gómez-Martín, M.E., Corredor, A., 2010. Influence of armour unit placement on armour porosity and hydraulic stability. Proc. 32nd Int. Conf. on Coastal Engineering, ASCE 1 (32), 41. https://doi.org/10.9753/icce.v32.structures.41 structures.

Medina, J.R., Molines, J., Gómez-Martín, M.E., 2014. Influence of armor porosity on the hydraulic stability of cube armor layers. Ocean. Eng. 88, 289–297.

Medina, J.R., Gómez-Martín, M.E., Mares-Nasarre, P., Odériz, I., Mendoza, E., Silva, R., 2019. Hydraulic Performance of Homogeneous Low-Crested Structures. Coastal Structures, Hannover (Germany, 30 Sept.-2 October.

Medina, J.R., Gómez-Martín, M.E., Mares-Nasarre, P., Escudero, M., Odériz, I., Mendoza, E., Silva, R., 2020. Homogeneous low-crested structures for beach protection in coral reef areas. Proceedings of virtual Conference in Coastal Engineering 36v papers.59.

Millington, I., 2007. Game Physics Engine Development. Elsevier, p. 481.

Moreau, J.J., 1999. Numerical aspects of the sweeping process. Comput. Methods Appl. Mech. Eng. 177 (3–4), 329–349.

Muttray, M., Reedijk, J., Vos-Rovers, I., Bakker, P., 2005. Placement and structural strength of Xbloc and other single layer armor units. In: Proceedings Int. Conf. On Coastlines, Structures and Breakwaters. Institution of Civil Engineers (ICE), London (UK), 20-22 April.

Odériz, I., Mendoza, E., Silva, R., Medina, J.R., 2018. Stability and Hydraulic Performance of Homogeneous Cubipod Low-Crested Mound Breakwater. In: Proceedings of the 7th International Conference on the Application of Physical Modelling in Coastal and Port Engineering and Science (Coastlab18). Santander (Spain), May 22-26.

Özkan-Çevik, E., Cihan, K., Yüksel, Y., 2005. Stability for structures armored with Core-Loc. Turk. J. Eng. Environ. Sci. 29 (4), 225–233.

Pardo, V., Herrera, M.P., Molines, J., Medina, J.R., 2014. Placement test, porosity and randomness of cube and Cubipod armor layers. J. Waterw. Port, Coast. Ocean Eng. 140 (5).

Radjai, F., Richefeu, V., 2009. Contact dynamics as a nonsmooth discrete element method. Mech. Mater. 41 (6), 715–728.

Rinkewich, B., 2014. Rebuilding coral reefs: does active reef restoration lead to sustainable reefs? Current Opinion in Environmental Sustainability 7, 28–36.

Smith, E.R., Melby, J.A., 1998. Three-Dimensional Breakwater Stability Tests at Vale de Cavaleiros, CapeVerde. CHL-98-22, July 1998. USACE, Waterways Experiment Station.

U.S. Army corps of engineers, 1984. Shore protection manual, U.S. Army engineer waterways experiment station, coastal and hydraulics laboratory, vicksburg, MS.

Xiang, J., Latham, J.-P., Zimmer, D., Baird, W.F., Fons, M., 2011. Modelling breakwater armor layers and the dynamic response of armor units. Proceedings of International Conference on Coastal Structures, Yokohama (Japan) 1, 318–329. September 6–8.

Yagci, O., Kapdasli, S., 2003. Alternative placement technique for Antifer blocks used on breakwaters. Ocean. Eng. 30 (11), 1433–1451.